

Prominence and plage activity in the recently discovered late-type rapid rotator, RE 1816+541

M.T. Eibe*

Armagh Observatory, College Hill, Armagh BT61 9DG, Northern Ireland

Received 6 May 1998 / Accepted 30 June 1998

Abstract. The rapidly-rotating, chromospherically active late-type star RE 1816+541 has shown signs of intense magnetic activity in various forms. Time-series of high resolution spectra have been obtained during three nights and several important events were detected. Observations contained several chromospheric lines, allowing us investigate simultaneously the response of the chromosphere at different heights.

A detailed analysis of the $H\alpha$ line behaviour, in particular, has revealed prominence clouds and plage-like regions in this star. Rapid rotation favours detection and further investigation of these features. Prominence clouds are seen to lie below the co-rotation radius. A bright plage-like region was well resolved on the first night. The feature disappeared temporarily during meridian crossing, coinciding with the passage of a cloud. Complete obscuration of the plage by the cloud proves that the emission feature is located on or near the stellar surface, whereas the cloud is at larger height and is seen in projection onto it. A very large flare was also detected during the observations, having strong effects in all the chromospheric lines selected for study.

Key words: stars: activity – stars: chromospheres – stars: individual: RE 1816+541 – starspots

1. Introduction

The most extreme examples of magnetic activity phenomena are generally found in rapidly-rotating late-type stars. Current theories to explain the origin of magnetic phenomena are based on the interaction between plasma and magnetic fields. The two physical processes of convection and rotation are believed to play a fundamental role in the generation of stellar magnetic fields through a dynamo mechanism (Parker 1970). In this scenario rapid rotators among the convective, late-type stars are expected to show signs of stronger activity. This may be not valid, however, for stars at the bottom of the main sequence. Recent studies of rotation and activity in very late-type dwarfs (Basri & Marcy 1995) suggest a significant change in the rotation-activity connection for the latest-type stars.

Rapid rotation is also a very important factor in order to resolve and investigate spatial features in stars. High rotational velocities ensure that the chromospheric line profiles are rotationally dominated, favouring the detection of emission and absorption transients associated with plage and prominence phenomena, respectively.

Observations of RE 1816+541 were first aimed at seeking evidence for stellar prominences in this object, as part of a project to investigate the nature of this kind of phenomena. Although there are several examples of rapidly-rotating late-type stars showing signs of prominence activity (Cameron & Robinson 1989a,b; Collier-Cameron & Woods 1992; Jeffries 1993; Byrne, Eibe & Rolleston 1996), our understanding of stellar prominences and their possible implications is still poor. Detailed studies were carried out only in two well known cases: the K dwarf AB Dor (Cameron & Robinson 1989a,b) and the M dwarf HK Aqr (Byrne, Eibe & Rolleston 1996, Eibe 1997, van den Oord, Eibe & Byrne 1998, hereafter VEB98). Prominences in AB Dor occur near the co-rotation radius and may be formed as condensation at the top of magnetic loops that extend beyond this radius, where the effective gravity is directed outwards. This condensation mechanism constitutes the basis of a model proposed by Collier-Cameron (1988) to explain prominence clouds formation in rapidly-rotating stars. Under negative effective gravity, condensed material could dissipate by diffusion across the field lines, leading to stellar angular momentum loss. Consequently, it was first thought that prominence clouds could contribute significantly to AB Dor's rotational braking rate.

This result would have important implications for angular momentum evolution studies. Investigations by Stauffer et al. (1984, 1985) showed that rotational braking on G and K type rapid rotators of young open clusters occurred too rapidly to be explained by conventional angular momentum loss theories, via a stellar wind. It was therefore interesting to investigate whether prominence clouds could account for the observed spin-down time-scales. However, later work to estimate cloud masses and lifetimes in AB Dor (Collier-Cameron et al. 1990) implied that they would not be very efficient as a braking mechanism. Moreover, in recent work by Collier-Cameron & Jianke (1994) it is concluded that conventional wind models may be adjusted

Send offprint requests to: M.T. Eibe

* Present address: LAEFF, Apdo 50727, E-28080 Madrid, Spain

to explain the rotational evolution of G and K dwarfs in young clusters, without introducing new braking mechanisms.

Prominences in HK Aqr have turned to be fundamentally different to those found in AB Dor, since they have been mainly found well below the co-rotation radius. In this case it is not possible to apply Collier-Cameron's model (1988) and, additionally, the role of prominence clouds in rotational braking is also dubious.

By analysing further examples of late-type rapid rotators it is possible to obtain more observations of stellar prominences and discriminate between different models. Results may not only provide a more complete view of the phenomenon but also have important consequences in studies of angular momentum evolution.

The star RE 1816+541 is similar to HK Aqr in many respects. This paper contains the main results derived from an extensive analysis of its $H\alpha$ line variability. These include the study of prominence clouds and discrete bright regions, the latter being ascribed to solar-like plage regions.

2. RE 1816+541

RE 1816+541 has been discovered as the optical counterpart to a bright EUV source detected during the Wide Field Camera (WFC) All-Sky Survey phase of the ROSAT mission. From the Hubble Space Telescope Guide Star Catalog (Jenkner et al. 1990) the position and magnitude are $RA = 18^h 16^m 16^s.8$, $Dec = +54^\circ 10' 22''$ (J2000.0), $V=11.7$.

Medium and low resolution optical spectroscopy of this object was presented by Jeffries, James & Bromage (1994), who classed it as a single, rapidly-rotating dM1-2e star with a $v_* \sin i$ of 61 km s^{-1} . Assuming a main sequence radius, this corresponds to a period, $P_{rot} \sim 12 \sin i$ hrs or $0.5 \sin i$ d. A high level of activity is indicated by strong emission in $H\alpha$ and Ca II H & K, both commonly used as chromospheric indicators. Based also on its high EUV flux as measured by the WFC, RE 1816+541 is regarded as one of the most active stars in the solar neighbourhood. Arguments for a youthful evolutionary status, based on its rapid rotation and its kinematics, are given by those authors.

Mean magnitudes and colours of RE 1816+541 were given by Schwartz et al. (1995). Robb & Cardinal (1995) obtained differential photometry with the Johnson V filter. From the modulation of the light curve they derived a period of 0.459 d and concluded that the star has large active regions on its surface causing the brightness variations. In order to calculate rotational phases, we have used in this work the ephemeris given by those authors, $HJD=2449927.752 + 0.4589E$.

The combination of this period with $v_* \sin i$ gives a projected radius, $R_* \sin i \sim 0.55 R_\odot$. The absolute visual magnitude, M_V , is derived from the photometry published in Schwartz et al. (1995), $M_V=10.32$, assuming a distance of about 20 pc (Jeffries, James & Bromage 1994). Then, using the mass-visual luminosity relation for low-mass stars from Henry & McCarthy (1993), a mass estimate $M \sim 0.49 M_\odot$ is obtained. The stellar radius can be determined from calibrated mass-radius relations. According to the empirical mass-radius relation for late M dwarfs produced

Table 1. Log of the spectroscopic observations of RE 1816+541 taken with the WHT/UES on 25–27 June 1996. The start and end times of continuous sequences of spectra are recorded. Gaps of 15–20 min were due to the observations of B stars and another active late-type star which was studied as part of a different project. Phases (φ) have been calculated according to the ephemeris given in Robb et al. (1995), $HJD=2449927.752 + 0.4589E$

Date	JD (2450260+)		Phase	
	start	end	start	end
25 June	0.3905	0.6119	0.861	0.343
	0.6278	0.7277	0.378	0.595
26 June	1.3998	1.4687	0.060	0.210
	1.4836	1.5426	0.242	0.371
	1.5519	1.6271	0.391	0.555
	1.6333	1.7375	0.569	0.796
27 June	2.3940	2.4562	0.227	0.362
	2.4632	2.5223	0.377	0.506
	2.5390	2.6013	0.543	0.678
	2.6103	2.7328	0.698	0.965

by Caillault & Patterson (1990) the result is $R_* \sim 0.52 R_\odot$. This is in good agreement with the value predicted by the mass-radius relation for main-sequence stars given in Demircan & Kahraman (1991), $R_* \sim 0.52 R_\odot$. The latter relation was obtained using theoretical stellar models for ZAMS stars.

From comparison between the estimates of both R_* and $R_* \sin i$, it follows that the stellar inclination must be close to 90° . Combining the radius and mass estimates yields a co-rotation radius, $R_{corot} \sim 5.45 R_*$.

3. Observations and data reduction

RE 1816+541 was observed with the 4.2m William Herschel Telescope (WHT) at the Observatorio del Roque de los Muchachos on the island of La Palma (Canary Islands) between 25–27 June 1996, using the Utrecht Echelle Spectrograph (UES, Unger & Pettini 1993). UES was used in conjunction with a $31.6 \text{ lines mm}^{-1}$ grating and 1024×1024 pixels TEK $24 \mu\text{m}$ CCD. A 1.1 arcsec wide slit was used, which corresponds to two detector pixels and a resolving power $\lambda/\Delta\lambda$ of 55000 (FWHM). The spectra cover the wavelength region 5350–9231Å which was recorded in 45 orders, allowing simultaneous observation of the $H\alpha$ and Ca II IR³ emission lines. Because of the limited size of the detector it was not possible to fit the entire echellogramme. The resulting gaps between consecutive orders were of $\sim 8\%$ in the blue up to $\sim 59\%$ in the red end of the range. The integration time was set at 200 s. Time overhead between subsequent exposures was ~ 80 s, yielding a time resolution of ~ 5 min. A log of the observations can be found in Table 1.

The three nights of observations were clear. Meteorological conditions were generally stable. Spectra obtained on the second night were of somewhat poorer S/N due to the high winds. Best seeing conditions were achieved on the last night, 27 June,

with an average seeing disk, 1.1 arcsec. For the first and second nights, the average seeing was 1.4 and 1.3, respectively.

An adequate number of bias frames, flat frames and dark count exposures were taken at the beginning of each night. Th-Ar calibration lamp spectra were taken throughout the night to account for possible shifts of the wavelength calibration. Spectra were processed semi-automatically using standard packages within IRAF (Tody et al. 1986).

4. Calculation of the stellar velocity

4.1. Radial velocity

The radial velocity was measured in two different ways. First, by doing gaussian fits to a single, isolated photospheric absorption line (Fe I 6546.25Å) and, second, by applying a cross-correlation technique.

The main problems with determining accurate velocities from gaussian fits are the intrinsic line profile variability and the blending of photospheric lines due to a combination of rapid rotation and late-spectral type. The heliocentric velocity derived by using this method was $-24.8 \pm 2.8 \text{ km s}^{-1}$, a value which is close to that obtained by Jeffries, James & Bromage (1994), $-21.9 \pm 1.5 \text{ km s}^{-1}$. In both cases, the error is given as a standard deviation.

This result was confirmed by cross correlating individual spectra with the spectrum of HIC 67155, a non active star with a M3 spectral type, comparable to that of RE 1816+541. From the shift of the cross-correlation peak an average velocity of $-22.9 \pm 3.4 \text{ km s}^{-1}$ was derived. This does not include results from the data obtained during the last night since they gave much larger uncertainties and the quality of the cross correlation was considerably worse. For this reason, the value finally used to refer the spectra to the stellar rest frame was $-23.8 \pm 3.1 \text{ km s}^{-1}$, obtained as an average of the velocities from cross correlations for the first two nights and the velocity from gaussian fits to photospheric lines done on the last night.

4.1.1. Rotational velocity

As a measure of rotation, the $v_* \sin i$ has been calculated from cross correlation analyses, using again the spectrum of HIC 67155 as a template. In order to obtain a relationship between the width of the cross-correlation peak and $v_* \sin i$, the template spectrum has been broadened to different velocities. By cross-correlating the resulting spectra with respect to the unbroadened template spectrum, a width value was obtained for each velocity. The calibration between width and rotational velocity was then established by doing a linear least-squares fit to those points. The $v_* \sin i$ value obtained for RE 1816+541 is $62 \pm 5 \text{ km s}^{-1}$, in agreement with results found previously by Jeffries, James & Bromage (1994).

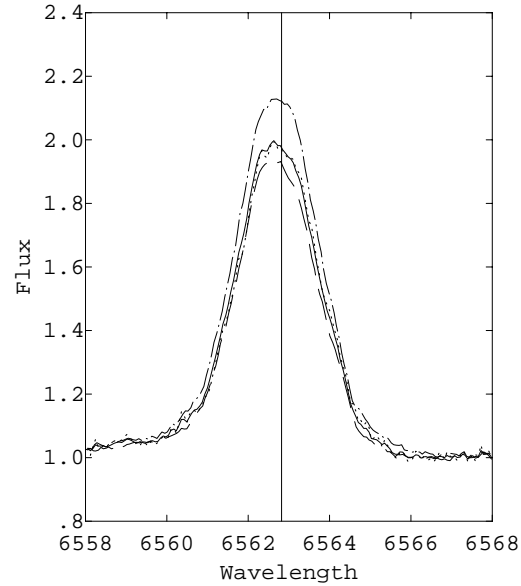


Fig. 1. The nightly mean H α profiles for the nights of August 25 (---), August 26 (...) and August 27 (-.-). Also shown is the overall mean profile (—) that was used in the analysis of the emission variability. The vertical line indicates the rest wavelength of H α

5. Variability of chromospheric emission

5.1. The H α emission line

The H α line was seen to vary rapidly with significant changes in both equivalent width and in line profile. The most pronounced variations occurred during the last night of observations. In Fig. 1 are shown the nightly mean profiles. The parameters of the gaussian functions that best fit these profiles are given in Table 2. Emission appears to be blueshifted by about $\sim -6 \text{ km s}^{-1}$ on the three nights. This, in principle, may indicate an overall rise of the chromosphere. However, as it will be seen later, there are numerous absorption and emission events that can also be contributing to the observed profile shape. For this reason, the symmetry/asymmetry of the mean profiles will not be discussed further. The mean level of emission is clearly lower on June 25 and considerably higher on June 27.

Proceeding as in Byrne, Eibe & Rolleston (1996), a search for systematic behaviour of the H α line was first done by looking at the ratios between all individual spectra and a mean *reference* spectrum. In this case the *reference* is an overall mean, made of a total of 242 spectra that were not affected by significant emission events. This profile is also shown in Fig. 1 (*continuous line*) for comparison. Its FWHM, 2.33Å, agrees well with the value predicted for rotational broadening, $\Delta\lambda_{rot} \sim 2.31\text{Å}$, suggesting that doppler broadening dominates over other sources of spectral line broadening.

Dynamic H α ratio spectra for each of the observing nights are shown in Figs. 2–4. Each line of a grey-scale image correspond to the ratio between an individual profile and the overall mean. Spectra are all displayed in a velocity scale relative to the stellar rest frame set at -23.76 km s^{-1} . This technique allows

Table 2. Parameters of the gaussian fits to the nightly mean H α profiles

Night	λ_0	EW(\AA)	FWHM(\AA)
June 25	6562.69	-2.29	2.31
June 26	6562.74	-2.38	2.32
June 27	6562.71	-2.74	2.34

to rapidly obtain information about the characteristic features that are determining the shape of the line profile as well as the specific velocities at which largest variability takes place.

Visual inspection of the dynamic H α ratio spectra indicates that in general the pattern of the line variability is different from night to night. Closer examination, however, reveals some common features. A narrow absorption transient is neatly defined in Fig. 2 between phases $\varphi \sim 0.2$ – 0.3 . This event appears to obscure completely the prominent emission feature that is seen to propagate from blue to red in the line profile between $\Delta\varphi \sim 0$ – 0.5 . Although they are less obvious, these two features recur on the following nights (see Figs. 3 and 4). Spectra taken on the night June 26 are of poorer quality, making detailed analysis of the profile more difficult. Unfortunately the phase coverage of the night June 27 was such that the early stages of those events were already missed when the series of observations began.

Signs of another absorption transient are detected at phases near $\varphi \sim 0.9$. Its existence is, however, more difficult to trace. On the night June 25 it appears to occur in connection with an additional redshifted component, manifested in Fig. 2 by the intense absorption seen in the red during phases $\varphi \sim 0.9$ – 0.1 . On the night June 27, observations finished at phase $\varphi \sim 0.96$ so that only the propagation of the absorption in the blue was recorded. Its presence was impossible to confirm on the night June 26 due to differences in phase coverage.

Evidence of a deep blueshifted absorption is also found at the end of the night June 25, emerging in the profile at $\varphi \sim 0.4$. Absorption events at these phases are also detected on the following nights but they exhibit a generally different behaviour.

An extraordinary event occurred on the night June 27. This is the most noticeable feature in Fig. 4. It starts as obvious blue-shifted emission ($\varphi \sim 0.6$) that propagates rapidly toward the red. A slow and gradual decay phase follows until extra-emission fades completely at $\varphi \sim 0.9$.

A more detailed study of these events will be deferred for a later section.

5.2. Other spectral lines

The dynamic spectra for the other interesting chromospheric lines which were observed have been constructed in the same way that in the case of H α and are shown in Figs. 5–8. These are used here mainly for comparison and more thorough description will follow in future work. In the case of the He I D₃ and Na I D-lines the images are made of individual spectra instead of ratios in order to improve contrast. The captions of the figures are as follows:

6. Analysis of the H α variations

Figs. 2–4 were used as a guide to trace significant features in the individual ratio spectra. Each of them was investigated by using the gaussian-fitting method that was previously followed in the case of HK Aqr (Byrne, Eibe & Rolleston 1996). Due to the complexity of the profiles, deblending fits were often necessary to resolve the contribution of different components. Results from this analysis are presented in this section.

6.1. Absorption features

As shown in Sect. 5.1, several absorption transients were detected in the course of the observations. They will be labeled with letters A, B and C for quick reference in the text. Transient A is the event that was seen to recur on the three nights between phases ~ 0.2 and ~ 0.3 . Transient B is the strong absorption feature seen near $\varphi \sim 0.5$, just prior to the major emission event on June 27. Finally, transient C corresponds to the very deep absorption detected near the start of the series on June 25, at phases $\varphi \sim 0.9$ – 0.1 . The possible recurrence of transients B and C on the three nights will be discussed below. Subscripts 25–27 will be used to indicate the corresponding night in each case.

The three absorption transients, which have been identified using the technique of dynamic spectra, are now analysed in more detail to check whether they can be explained in terms of prominence condensations of neutral material.

6.1.1. Transient A

Fig. 9 shows the results from gaussian fits to the well-defined absorption transient centred at phase $\varphi \sim 0.25$. Data from different nights are overplotted using different symbols: + for June 25, \square for June 26, and \triangle for June 27. The two horizontal lines in the RV diagram (*bottom panel*) indicate the projected rotational velocity, $\pm v_* \sin i$ ($v_* \sin i \sim 61 \text{ km s}^{-1}$). Changes in the radial velocity (RV), equivalent width (EW) and full width at half maximum (FWHM) appear to be correlated as the transient moves across the H α profile. Details of these variations are specified below:

1. The feature is seen at similar phases during at least three nights ($\Delta\varphi \sim 0.20$ – 0.29 on the night of June 25, $\Delta\varphi \sim 0.18$ – 0.29 on the night of June 26, $\Delta\varphi \sim 0.23$ – 0.28 on the night of June 27). The phase coverage in June 27 made it impossible to detect the complete transit on that night.
2. Agreement between different nights is especially good in RV, except for the slightly more redshifted velocities measured on June 26 between $\varphi \sim 0.18$ and $\varphi \sim 0.21$. According to the pattern of the EW variations, however, the absorption appears stronger on the first night.
3. The EW increases rapidly as the feature appears in the blue wing of the profile and continues to move redwards. Absorption gets again weaker at larger positive velocities.
4. A sharp peak of EW occurs near $\varphi \sim 0.21$. At this time the central position of the feature is shifted to the blue. The pat-

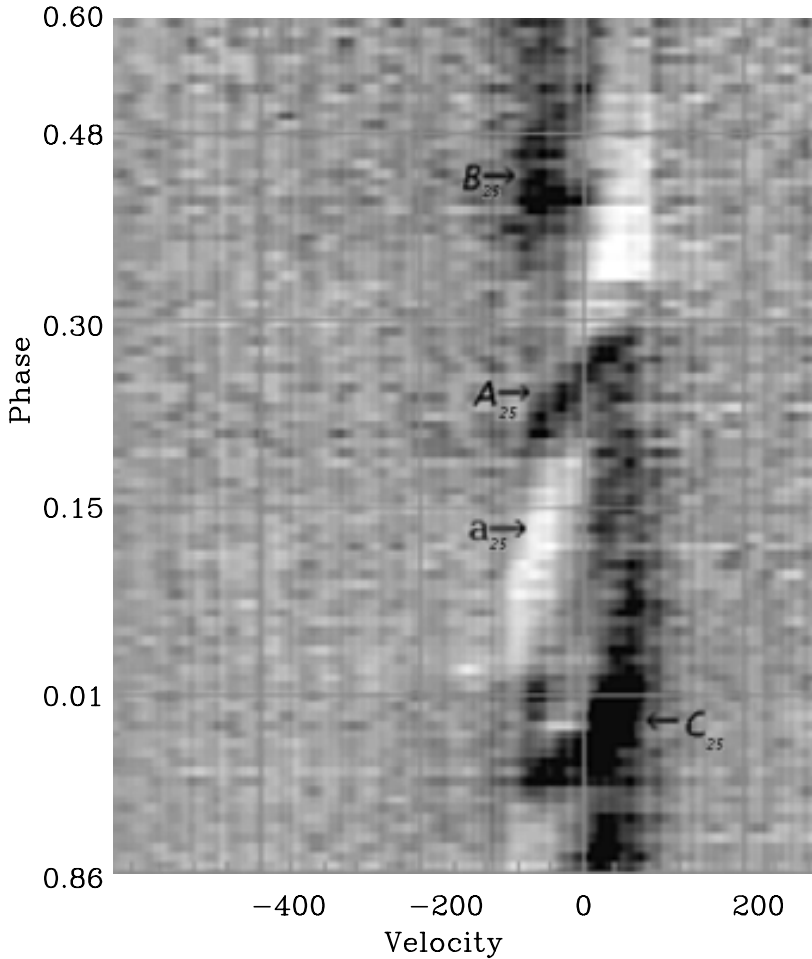
Dynamic spectrum of H α on June 25

Fig. 2. Dynamic spectra of H α on June 25. The grey-scale image is made of ratio profiles that result after dividing by the overall average. Rotational phases are indicated in the left edge and the velocity scale in the horizontal axis is referred to the stellar rest frame, set at -23.76 km s^{-1} .

tern of the EW variations is therefore asymmetric, increasing more quickly than it is seen to decline.

5. The FWHM variations show a larger scatter. The feature is generally narrow ($\Delta\lambda_{FWHM} \sim 1-1.5$) but broadens considerably near $\varphi \sim 0.21$, coinciding with maximum EW. In any case, it is much less than expected for rotational broadening, $\Delta\lambda_{rot} \sim 2.31 \text{ \AA}$.
6. The central position of the feature varies linearly with phase, moving from blue to red, in an interval of phase $\Delta\varphi \sim 0.1$.
7. When observed, the extreme velocities are not perfectly symmetric about zero but systematically blueshifted by $\sim 20 \text{ km s}^{-1}$.

6.1.2. Transient B

This feature is seen clearly in Fig. 4 (B₂₇). It appears at $\varphi \sim 0.36$ as a relatively weak ($EW \sim 0.03 \text{ \AA}$), narrow absorption ($FWHM \sim 1.05 \text{ \AA}$), blueshifted by about -20 km s^{-1} with respect to the stellar rest frame. It rapidly propagates towards the red, increasing in depth and width before disappearing with the start of a strong flare. Its mean EW and FWHM during the last phases ($\Delta\varphi \sim 0.54-0.62$) are, respectively, 0.10 \AA and 1.90 \AA , substan-

tially higher than when seen in the blue. Fig. 4 suggests the presence of two maxima of absorption at this time. One appears to be fixed at 65 km s^{-1} while the other is slightly more to the blue but is more variable and propagates slowly to the red until both features finally merge together. Individual ratio profiles for these phases are shown in Fig. 10. It can be seen that the broad absorption component has often two peaks suggesting a possible blend between two individual features whose contributions are difficult to assess. In addition, simultaneous emission is seen in the blue at these phases with important effects in the profile, which may result in larger uncertainties in the velocities measured from gaussian fits. Evidence of absorption at these phases is also found on the other two nights (B₂₅ and B₂₆ in Figs. 2 and 3, respectively) but with different behaviour. B₂₅ is seen as strong absorption ($EW \sim 0.2 \text{ \AA}$) at $v \sim -50 \text{ km s}^{-1}$ and shows little variation with phase. Its appearance, however, may be influenced by the presence of additional emission in the red wing due to the effect of an emission transient as described in Sect. 6.2. The observed behaviour of B₂₆ is more similar as in this case the absorption is seen to cross the profile from blue to red. The feature is not so clear and measurements are less accurate due to the poorer signal-to-noise. It is interesting that the

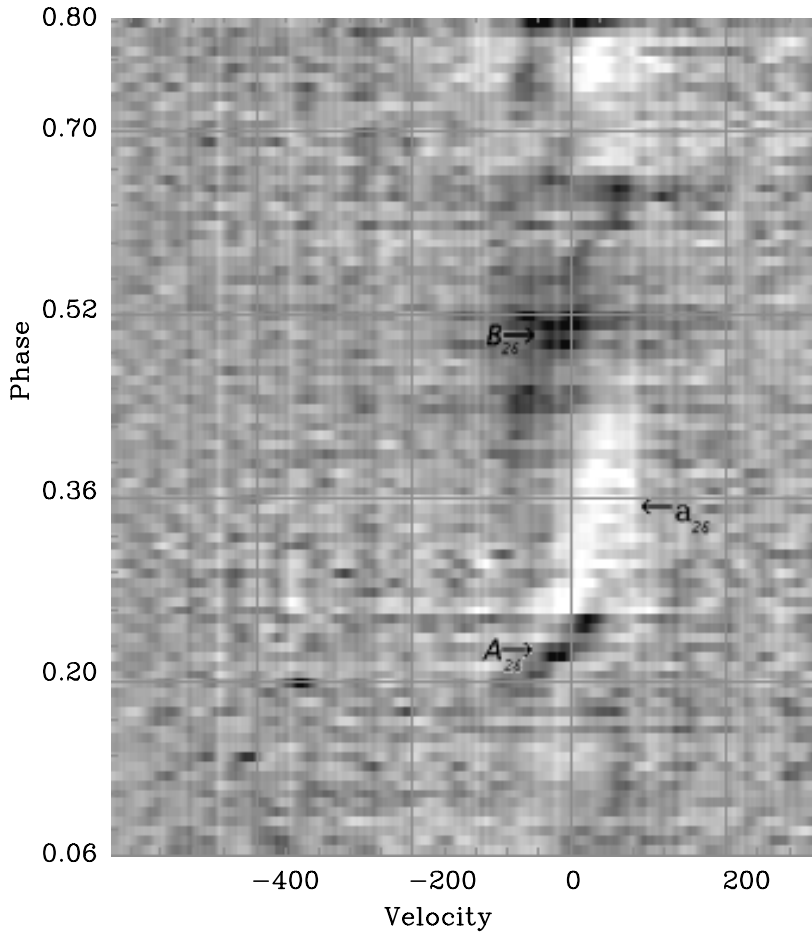
Dynamic spectrum of H α on June 26

Fig. 3. As Fig. 2 but for the night of June 26.

extreme radial velocities at the beginning and end of the transit ($\varphi \sim 0.4$ and $\varphi \sim 0.67$, respectively) are symmetric with respect to zero velocity, being the amplitude of the variations close to 50 km s^{-1} .

6.1.3. Transient C

From Fig. 2 it is seen that transient C_{25} is one of the strongest absorption events observed in RE 1816+541. It shows a complex morphology due to the concurrence of several features in the profile, making an unique interpretation of its evolution more difficult.

Two discrete components are seen during the onset of the event ($\varphi \sim 0.9$): an already present redshifted absorption at an average velocity of about 10 km s^{-1} and a blueshifted absorption by $\sim -60 \text{ km s}^{-1}$, that is moving towards the red. Both features are strongly blended at $\varphi \sim 0.96$, resulting in a very broad and deep absorption centred at about 10 km s^{-1} . A sudden brightening is seen in only one spectrum at $\varphi \sim 0.98$ and is followed by the appearance of a weak blueshifted absorption. Note that a bright transient (see below) is developing at this time so that the blueshifted absorption is seen superimposed on the blue emis-

sion wing. The absorption component in the red becomes more prominent for about 30 min ($\Delta\varphi \sim 0.04$) with an average width of about 2.3 \AA , close to the expected rotational broadening. It fades at $\varphi \sim 0.1$ but it remains visible in the red, before merging into transient A at $\varphi \sim 0.3$.

Unfortunately, differences in phase coverage do not allow to confirm the same kind of variations on the other two nights. At the end of June 27 ($\varphi \sim 0.93$), however, there is evidence for a well defined absorption at -80 km s^{-1} that propagates rapidly to the red (C_{27} in Fig. 4). On the other hand, weak absorption in the red between $\varphi \sim 0.1$ – 0.2 was also observed on June 26 (C_{26} in Fig. 3). If associated to the same event, the main part of its evolution could have been missed because the series of observations on this night started in fact at $\varphi \sim 0.06$.

6.2. Emission features

The bright emission transients seen in the H α line have also been analysed in order to investigate their origin and their possible connection to the absorptions. From Figs. 2–4 two major features can be distinguished: a discrete emission seen between phases $\varphi \sim 0$ – 0.5 on the three nights (transient \mathfrak{A}) and a very

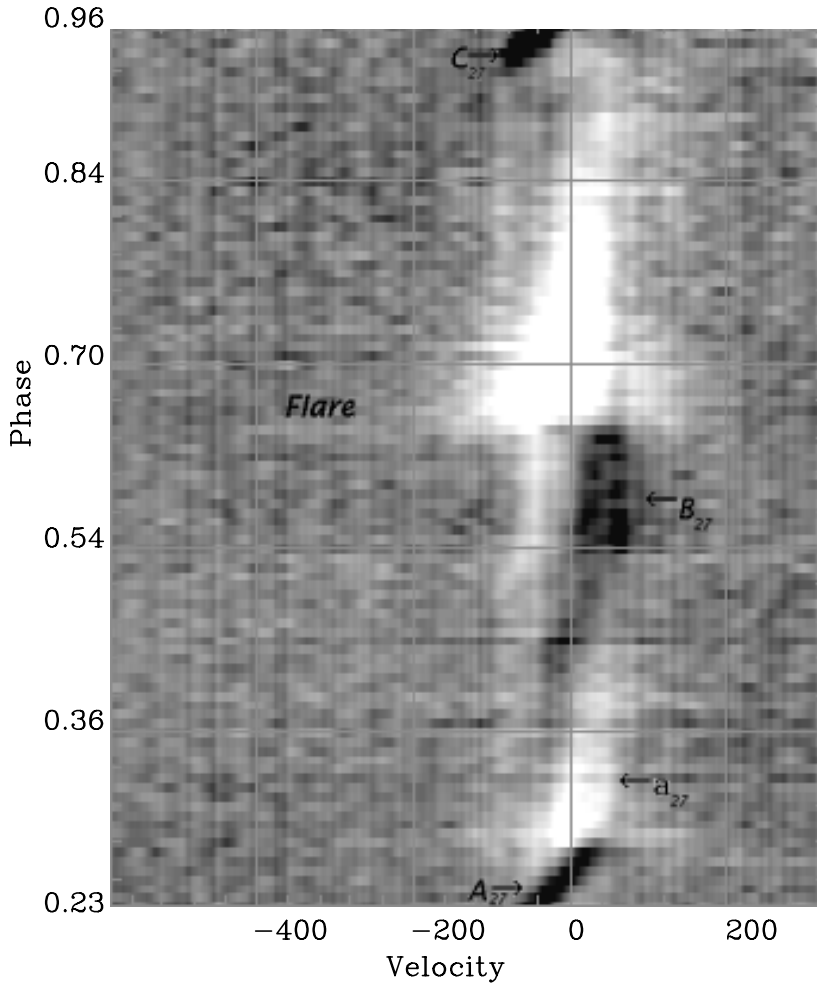
Dynamic spectrum of H α on June 27

Fig. 4. As Fig. 2 but for the night of June 27.

strong emission event that develops between $\varphi \sim 0.6$ – 0.9 on June 27.

6.2.1. Transient a

This feature is seen most clearly on the night of June 25 (a_{25} in Fig. 2). Although in less detail, it can also be identified on the other two nights (a_{26} and a_{27} in Figs. 3 and 4, respectively). On June 27 only the closing phases were covered. Results from a gaussian-fitting analysis are presented in Fig. 11. A summary of the most important properties revealed by this method is given below:

1. The whole event covers at least a phase interval of $\Delta\varphi \sim 0.5$.
2. The feature disappears temporarily between phases 0.2 and 0.3, coinciding with the passage of the absorption transient A.
3. Its width is narrower than expected from the rotationally broadened stellar profile, its FWHM being of the order of 1.22\AA .
4. The RV changes from blue to red within the entire episode and behaves almost linearly with time. Large deviations from linearity occurred near $\varphi \sim 0.2$ and also at the red end of the curve obtained on June 25.
5. The velocity amplitude exceeds $v_* \sin i$ of the star.
6. Extreme velocities are not symmetric with respect to zero velocity. On June 25 the RV was seen to change from $\sim -82 \text{ km s}^{-1}$ to $\sim 50 \text{ km s}^{-1}$. The extreme velocities observed on June 26 were $\sim -67 \text{ km s}^{-1}$ in the blue and $\sim 75 \text{ km s}^{-1}$ in the red, but at this night the opening phases of the event were missed.
7. Variations in EW are less pronounced. There is a trend of brightening at the closing phases on June 25 ($\varphi \sim 0.4$). A sudden brightening of the feature at the end of its passage across the disk is also observed on June 27. Unfortunately, earlier phases of the event were not covered on this night.
8. The phenomenon persists during three nights.

Dynamic spectra of CaII (8498 Å) on June 25 and June 27

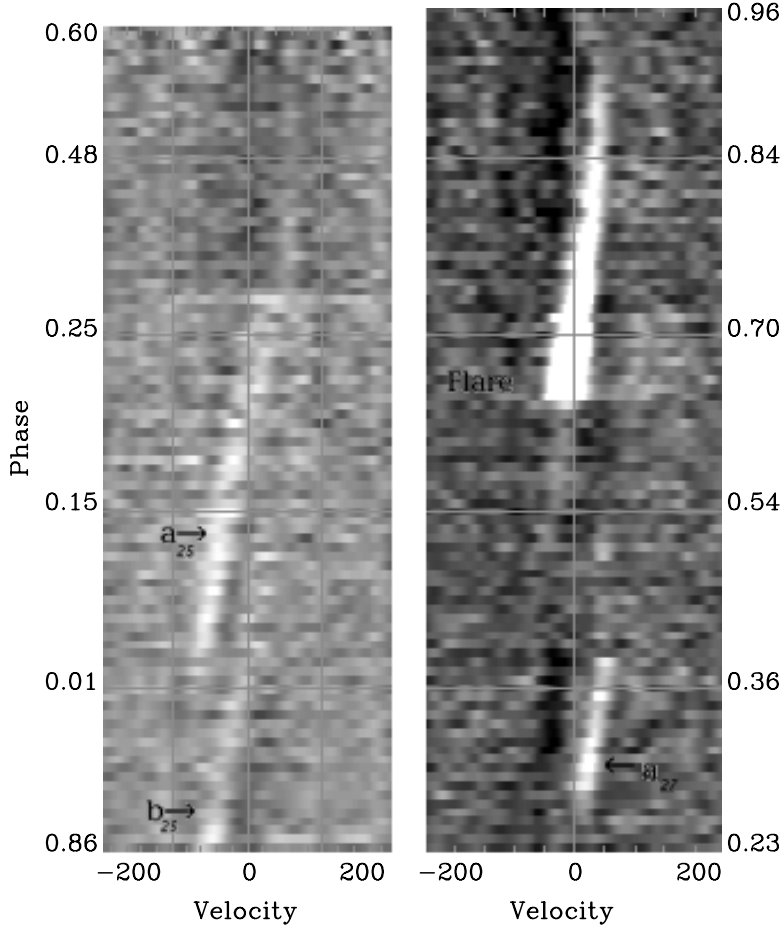


Fig. 5. Dynamic ratio spectrum of Ca II 8498Å on June 25 (*left*) and June 27 (*right*).

6.2.2. The strong emission on June 27

An extremely strong emission feature is clearly seen in the H α dynamic spectra of June 27 (see Fig. 4), starting near $\varphi \sim 0.6$ but extending over ~ 3.7 hrs. This is associated with a large flare that manifests dramatically in all the other chromospheric lines selected for study (see Figs. 5–8), implying it affected both above and below the temperature-minimum region. One of its most conspicuous aspects is the way it grows rapidly towards the red after emerging in the blue wing of the H α profile. This flare will be the subject of further investigation in future work.

7. Discussion

7.1. Prominence clouds

The observed evolution of transient A reminds that of the absorption features detected in the case of HK Aqr (Byrne, Eibe & Rolleston 1997). It agrees well with the expected behaviour of a prominence co-rotating cloud during its transit across the stellar disk. An estimate of the cloud location in the stellar atmosphere can be derived from the observed variation of its radial velocity. This has been done by following a specific formulation developed by VEB98. In that work it is shown how to estimate

the possible heights and latitudes for a co-rotating cloud, on the basis of its radial velocity evolution with time and period of visibility in front of the stellar disk. A brief outline of the method is given below in order to introduce some parameters that are going to be discussed later. For more detailed description the reader is referred to VEB98.

VEB98 assume that the absorption transients are caused by ideal, point-like clouds in the stellar atmosphere and thus ignores possible effects due to their sizes. In addition, the motion of the clouds is restricted by the condition of co-rotation with the star at some fixed distance above its surface, i.e. the system is rotating as a rigid body. Constraints on the cloud height (R_c) and co-latitude (θ_c) can then be derived from the variation of its measured radial velocity (v) with time. This should be linear when the cloud is seen near disk centre, verifying:

$$\left(\frac{dv}{dt}\right)_{(\varphi=0)} = \Omega^2 R_c \sin i K^{-1}, \quad (1)$$

where Ω is the stellar angular velocity and φ is the cloud's spheric coordinate, $\varphi = \Omega t$. The origin of φ is set at the stellar disk centre. K is defined as $K := \frac{R_c}{R_*} \sin \theta_c$, which is a constant quantity for a given cloud. The K value may be, therefore,

Dynamic spectra of CaII (8662 Å) on June 25 and June 27

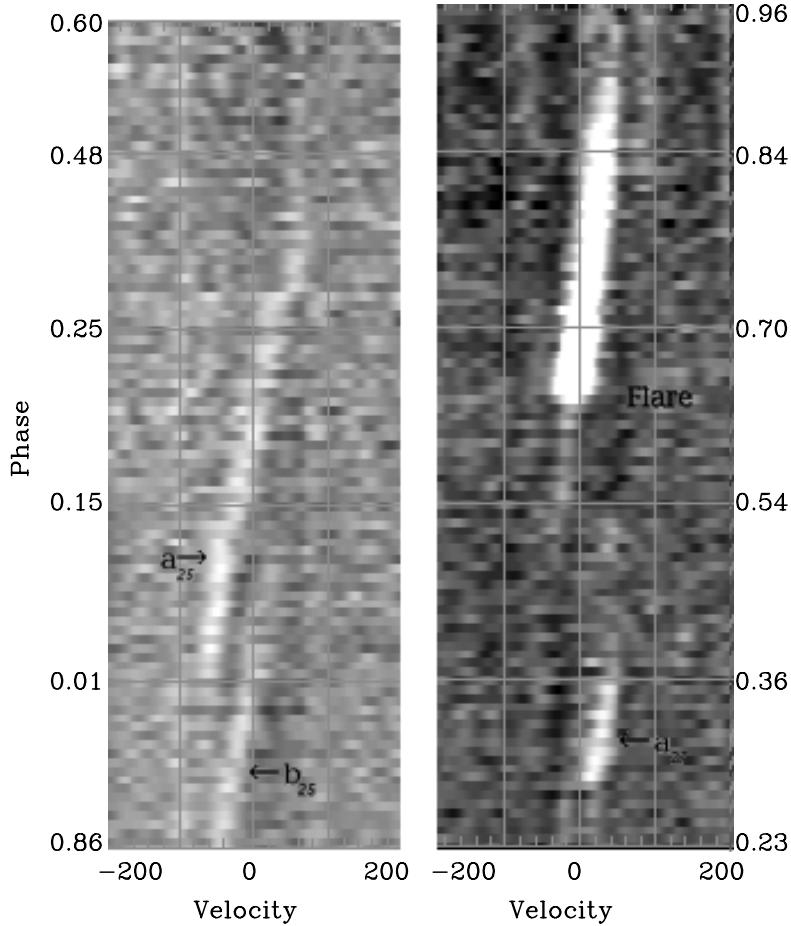


Fig. 6. As Fig. 5 for the Ca II 8542Å line.

estimated from the observed radial velocity evolution and is used to derive some limits for R_c and θ_c .

In order to detect the cloud in absorption, its projected position must be within the stellar disk. For a given inclination of the star, this only occurs for certain combinations of R_c and θ_c , thus providing a second relation to estimate the location of the cloud.

Analytically, it is impossible to determine independently both values, R_c and θ_c . VEB98 introduced a contour technique which allows to constrain them from the observations. Contours of K as a function of R_c and θ_c will be used here in order to establish limits.

The other absorption transient events appear to show more complex behaviour and are re-examined to see whether they can also be associated to similar phenomena.

7.1.1. The cloud detected as transient A

Fig. 9 shows the radial velocity variations observed on each night. Linear least-squares fits to the data are presented in Fig. 12. Results for different nights are in generally good agreement. Peculiar to the June 26 observations is the systematic

redshift that was found in the first five velocity measurements. This would affect significantly the results of the fit. From Figs. 3 and 9 it is seen that the absorption appears weaker at this time, being more difficult to detect. It is not possible to determine whether this is just an effect of the lower signal-to-noise of the observations at that night or it represents a real variation, perhaps due to a larger influence of the emission in progress (see Sect. 6.2). In any case those points were not included in the fit. The crucial values for the treatment that will follow are those close to zero velocity.

The results from these fits are listed in Table 3. It can be seen that the parameters derived from the different nights are consistent and agree extremely well within the calculated errors. Ingress and egress occur within a short fraction of the rotational period, suggesting the feature is at a considerable distance above the surface if in rigid rotation with the star. Clearly it must be over the bright transient that has been fully described in Sect. 6.2.1 as the discrete propagating emission is completely obscured at these phases.

Assuming an inclination of 90° , constraints on the height and latitude of the cloud are set by applying the method developed by VEB98, which has been briefly outlined above. The

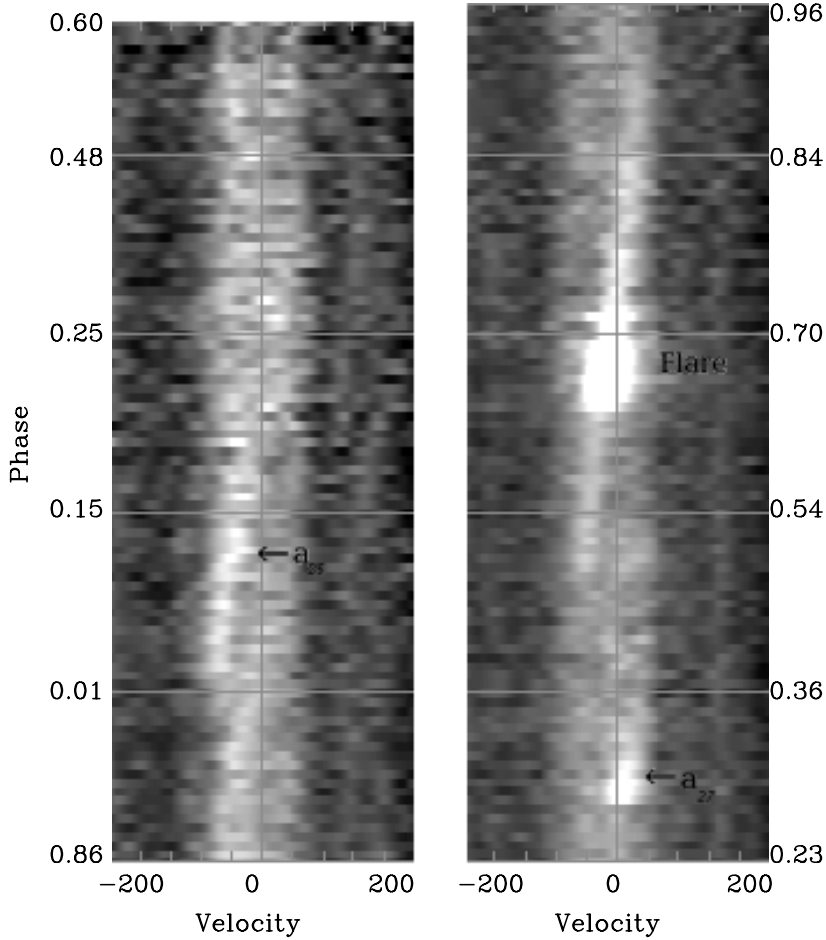
Dynamic spectra of He I D₃ on June 25 and June 27

Fig. 7. Dynamic spectrum of He I D₃. Individual spectra are shown instead of ratios in order to improve contrast.

Table 3. The main parameters of the cloud identified as transient A.

Date	dv/dφ	K	ΔK	Phase	
				Ingress	Egress
June 25	1494.401	0.256	0.011	0.197	0.289
June 26	1414.235	0.271	0.023	0.181	0.286
June 27	1533.895	0.250	0.013	(missed)	0.277

average of the three K values in Table 3 is used to determine the K -contour corresponding to the cloud in the $\theta_c - R_c$ diagram shown in Fig. 14. This diagram indicates the domain of possible heights (R_c/R_*) and co-latitudes (θ_c) for the co-rotating cloud detected as transient A (*thick solid line contour*). Limits to the cloud coordinates, R_c/R_* and θ_c , can also be derived analytically for an inclination of 90° applying the formulae derived in VEB98. Results obtained in this way are $3.86 \pm 0.34 \leq R_c/R_* \leq 3.99 \pm 0.33$ and $0.968 \leq \sin \theta_c \leq 1$ or, equivalently, $\theta_c \sim 75-90^\circ$, for the northern latitude solution. In any case, the cloud is found to be well below the co-rotation radius, but at a very large distance compared to solar prominences.

The location of cloud A suggests interesting aspects related to the clouds formation and stability. First, the cloud latitude is reasonably constrained and not far away from the equatorial plane. This may constitute an important condition favouring prominence formation. VEB98 investigated the mechanical forces governing the equilibria of neutral material confined in the stellar magnetic field at some height above the chromosphere of rapidly-rotating stars. In their analysis it is assumed that at sufficiently large distances from the star, the effective component of the magnetic field is the dipole component. Under this assumption it is found that force equilibrium on a field line is possible only in the equatorial plane. Second, the fact that cloud A lies below the co-rotation radius is also consistent with the picture obtained in the case of the rapidly rotating late-type star, HK Aqr (Byrne et al. 1996, VEB98). Therefore, the prominence formation mechanism invoked in Collier-Cameron's model (1988) must be excluded in these cases.

In their review of quasi-static coronal loop models, van den Oord & Zuccarello (1996) show that loops having a temperature inversion at their apices can also be generated by decreasing the heating at the summit or increasing their cross-sectional area.

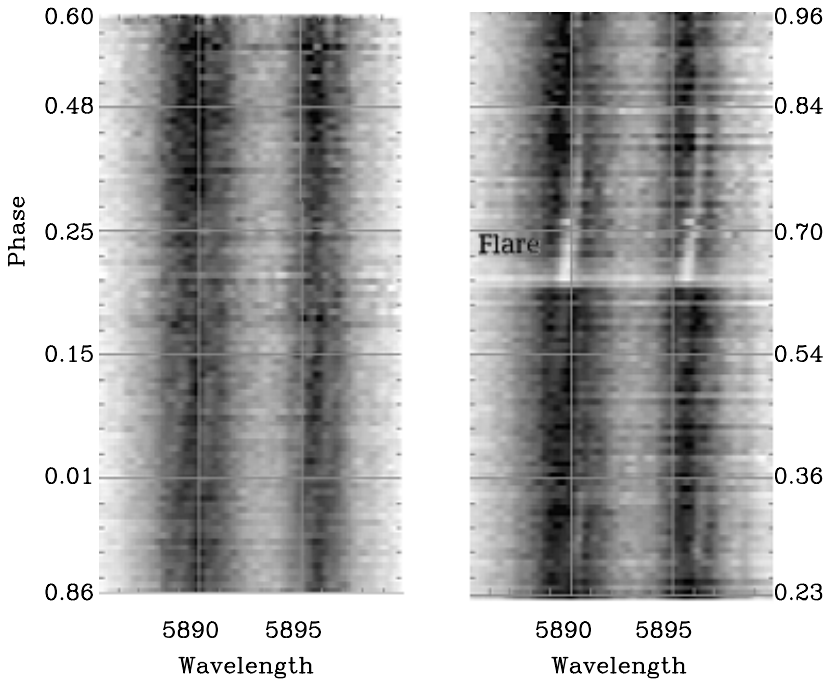
Dynamic spectra of NaI D_{1,2} on June 25 and June 27

Fig. 8. As Fig. 7 for the Na I D-lines.

In this new scenario, however, temperature reversals are not restricted to heights above the co-rotation radius.

Finally, evidence for this cloud is not found in any of the other chromospheric lines, which prevents further investigation of the physical conditions of the plasma contained in the prominence. In particular, with the H α observations alone it is impossible to determine both the kinetic temperature and the turbulent velocity from the line-broadening.

7.1.2. Transient B

Transient B is very interesting because of its apparent variation from night to night. The fact that it is seen as a deep and blueshifted absorption on the first night could imply material is moving outward with significant mass loss for the star. Its behaviour on the second night is in better agreement with the symmetric track followed by a co-rotating source while on the last night it becomes more enhanced in the red, suggesting receding absorbing material in front of the stellar disk. If due to a circumstellar structure, it could not be very high in the atmosphere as inferred from the relatively long disk-crossing time. In addition, from Fig. 3 it is seen that B₂₆ shows less contrast than A₂₆ against the concurrent emission component in the red. This may be due to changes in plage brightness and/or differences between the absorbing power of both transients. However, care must be taken when speculating about these possibilities since the signal-to-noise ratio on the night of June 26 is lower.

The amplitude of the radial velocity of transient B is very hard to estimate due to simultaneous excess emission in the profiles. However, based on the striking symmetry of the velocity track exhibited on June 26 with an approximate amplitude of

50 km s⁻¹, an estimation of its latitude was derived assuming a surface feature. In this case,

$$RV_{max} = v_{rot} \sin i \cos \lambda$$

where λ is the latitude of the feature and RV_{max} is the amplitude of its radial velocity. Therefore, an amplitude of 50 km s⁻¹ would imply a latitude, $\lambda \sim \pm 35^\circ$.

Fig. 13 shows the results obtained in an attempt to determine the radial velocities from gaussian fits to the H α ratio profiles. The crosses are for measurements on June 26 and the circles are for June 27. It can be seen that on June 27 the velocities are systematically redshifted and scatter increases towards the end of the event, presumably due to blending of more than one component as suggested above. Points for the other night correspond to the main component resolved in the profiles, which has been identified by comparison with Fig. 3 (B₂₇). Also shown in Fig. 13 are the straight-line fits to the data. A considerable change of slope between the two nights is obvious. If the transient was interpreted in terms of one and the same feature, this would indicate either some variation in height or the development of velocity fields between the two nights.

If the information from the linear fits and the observed phases of ingress and egress was used to estimate the location of such a feature according to the model of a co-rotating point source, one would find the following. The observations on June 26 are consistent with a cloud that co-rotates with the star at a relatively small height, $\sim 1.40\text{--}1.72R_*$. The data from the following night implies, however, a lower height, in the range $0.88\text{--}1.33R_*$. The domain of allowed heights and latitudes in both cases is represented graphically in Fig. 14.

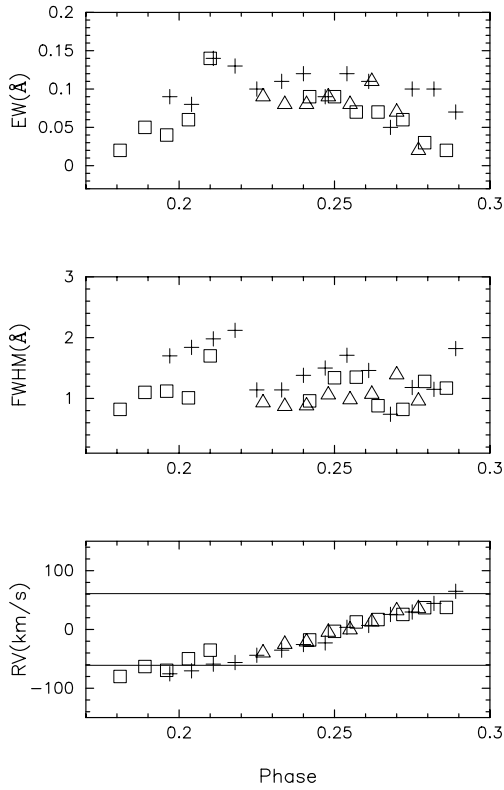


Fig. 9. Results from the gaussian fits to the transient A seen between phases 0.2 and 0.3 on the nights 25 June (+), 26 June (□), 27 June (△). The two horizontal lines in the RV diagram (*bottom panel*) correspond to the maximum Doppler shift associated to the projected rotational velocity

A possibility that comes to mind to explain the observed evolution of transient B is that it represents the development of a low-lying prominence-like structure. In this scenario the systematic blueshifts and redshifts observed on June 25 and June 27, respectively, may be indicative of the velocity fields involved in the formation of prominence clouds. For comparison, the escape velocity of the star at the surface is $\sim 600 \text{ km s}^{-1}$.

7.1.3. Transient C

The behaviour of transient C appears to be more complex and is harder to interpret. On June 25 (C_{25} in Fig. 2) the initial concurrence of blueshifted and redshifted absorption components in the profile suggests the simultaneous occurrence of both up-flows and downflows of material in the line-of-sight. In particular, the emission enhancement that is observed to precede the blueshifted absorption at $\varphi \sim 0.98$ supports an interpretation based on mass-loss events. As described in Sect. 6.1.3, the specially strong absorption that is seen in the red at these phases may actually consist of two components merged into one. It is important to note that in this case the reliability of the velocities from gaussian fits is more doubtful due to possible effects caused by the superposition of bright emission and redshifted absorption in the profile.

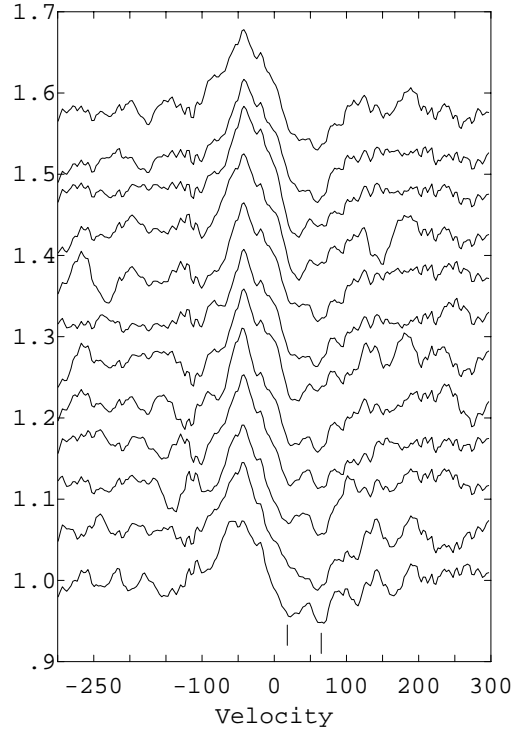


Fig. 10. Series of individual ratio profiles between $\varphi \sim 0.5\text{--}0.6$ on the night of June 25. The first spectrum is the one shown at the bottom and the following are shifted upward for clarity. The time between subsequent spectra is $\sim 5 \text{ min}$ ($\Delta\varphi \sim 0.007$)

On the other hand the propagating feature partially observed on June 27 near the same phases (C_{27} in Fig. 4) argues for the possible presence of a more stable co-rotating structure. As it occurred near the end of the series only six spectra could be obtained. Velocities measured by fitting gaussians to the absorption fit well in a linear curve going from ~ -85 to $\sim -27 \text{ km s}^{-1}$. If this was interpreted as a co-rotating cloud it would be at a height close to $4R_*$. More observations are required to confirm the nature of this transient.

7.2. Plage activity

Some of the observational facts summarised in Sect. 6.2.1 for transient **a** can be explained in terms of discrete bright regions close to the surface of RE 1816+541, which are ascribed to solar-like plages.

First, the small velocity width of the emission suggests it may arise in a localised centre of activity on the stellar surface. The duration of the transient and the observed radial velocities are consistent with this view. Detection of the feature on three successive nights indicates also that the phenomenon seen is not associated to an ephemeral brightening but to longer-lived structures. Finally, the interruption of the emission event by the prominence cloud provides additional support for the idea that the emission feature is located on or near the stellar surface, whereas the cloud is at a greater height and is seen in projection onto it.

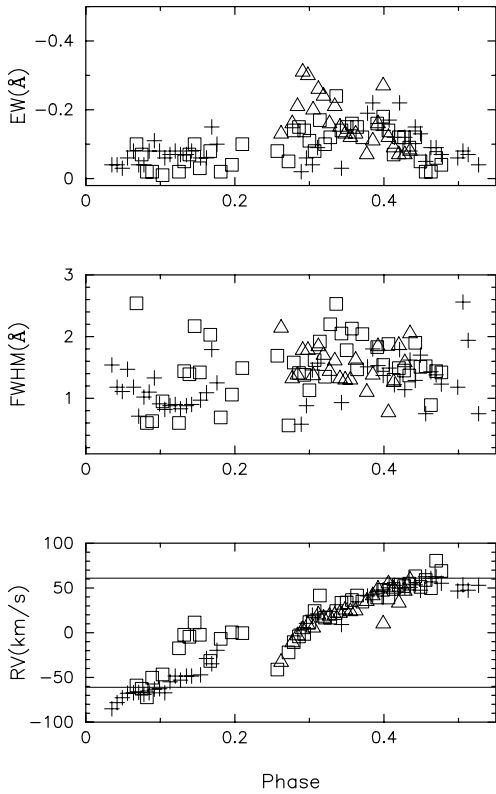


Fig. 11. Results from the gaussian fits to the emission feature a, seen between phases 0.0 and 0.5 on the nights of 25 June (+), 26 June (□), 27 June (△). The two horizontal lines in the RV diagram (*bottom panel*) correspond to the maximum Doppler shift associated to the projected rotational velocity

The velocity variations of the plage can be used to determine its location, following a similar method to that derived for the study of prominence clouds (VEB98). The major difference in this case is that a bright structure does not have to be in projection on the disk to be detected. If the emission region is at some height above the surface, its associated feature should still be visible outside the stellar disk and at velocities exceeding $v_* \sin i$.

The linear least-squares fits to the radial velocity variations are shown in Fig. 15. Cloud parameters derived from these fits are shown in Table 4. Note that the plage was not visible at zero velocities, when it is supposed to cross the centre of the disk, due to occultation by a prominence cloud at larger heights. Measurements done near those phases are more uncertain and were not included in the fits. Although a linear approximation of the RV as a function of time is less reliable near ingress or egress, those are unfortunately the only data available.

The diagram in Fig. 16 shows the range of possible heights and latitudes for the plage, as determined by using the K -contours on each of the two nights' data providing a good coverage of its transit across the disk. In this plot, heights are shown in units of the stellar radius. It is seen that results for the two nights are in good agreement.

In Fig. 15 the linear fits and the data points are compared with the radial velocity curves predicted for plages located within

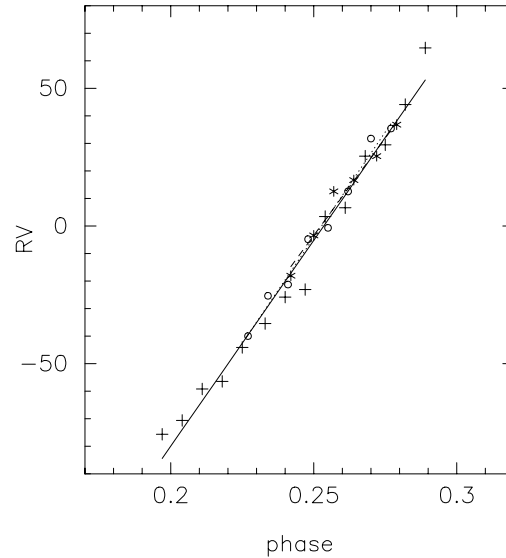


Fig. 12. Observed variation of the cloud (transient A) radial velocity (RV) with phase for the nights 25 June (+), 26 June (*), 27 June (o). The straight lines are the linear fits: 25 June (—), 26 June (---), 27 June (-.-). See text for a definition of parameters

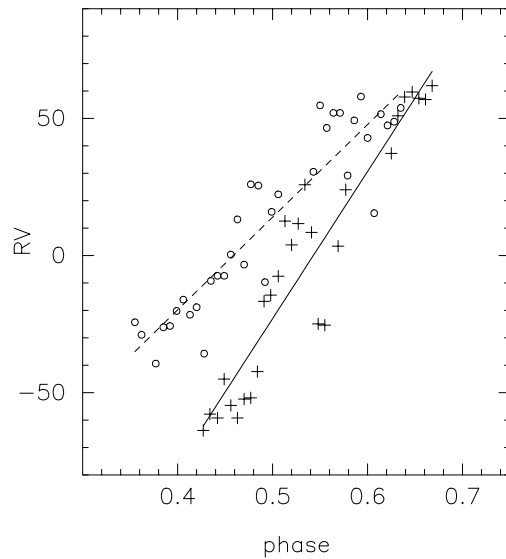


Fig. 13. Observed variation of the transient B radial velocity (RV) with phase for the nights 26 June (+) and 27 June (o). The straight lines are the linear fits: 26 June (—), 27 June (---)

the limits derived above and centred at $\varphi \sim 0.25$. These were computed on the assumption that the plage can be described by a point source of emission in co-rotation with the stellar surface, at height R and co-latitude θ . In this case its radial velocity (RV) is given by (see Sect. 7.1):

$$RV(t) = \frac{R}{R_*} v_{rot} \sin i \sin \theta \sin \varphi$$

Three cases are considered varying R and θ within the limits derived above:

- (1) $R=1.0R_*$, $\theta=50^\circ$ (*curve 1*)

Table 4. The main parameters of the plage (transient **a**)

Date	$dv/d\varphi$	K	ΔK	$R_{c,min}/R_*$	$R_{c,max}/R_*$	$\sin\theta_{c,min}$	$\sin\theta_{c,max}$
June 25	331.772	1.155	0.031	0.86 ($\equiv 1$)	1.32	0.654	0.866
June 26	320.580	1.196	0.044	0.84 ($\equiv 1$)	1.30	0.641	0.836

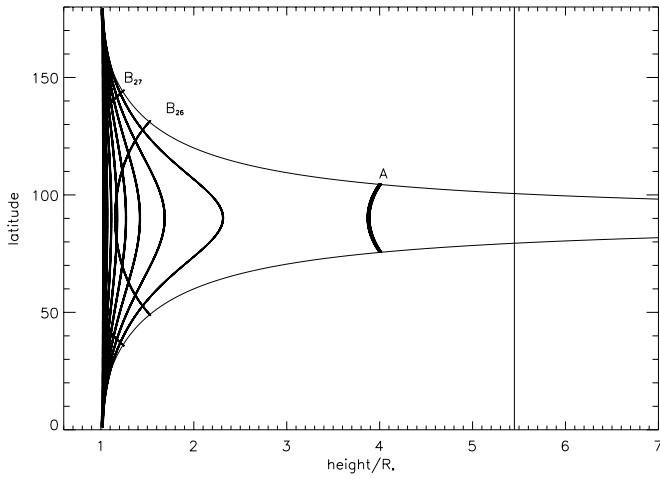


Fig. 14. Diagram showing the estimated position of the cloud associated to transient **A** (*thick solid contour*) and the ones that would correspond to transients **B₂₇** (*left thin contour*) and **B₂₆** (*right thin contour*). Note that if the interpretation in terms of a co-rotating point-like model for this feature is valid, a significant change of height between the two nights would have taken place. To construct this diagram an inclination of 90° was assumed (see Sect. 2). The thin vertical line marks the position of the co-rotation radius in the equatorial plane. See VEB98 for more details on the interpretation of this diagram

- (2) $R=1.0R_*$, $\theta=60^\circ$ (*curve 2*)
- (3) $R=1.3R_*$, $\theta=50^\circ$ (*curve 3*)

These fits cannot reproduce the observed asymmetry in the extreme radial velocities. An asymmetry effect could derive from intrinsic motion of the emission source. It could also result from temporary activation of the plage region at some phases (see below). On the other hand, the fit corresponding to the first night's data suggests a phase shift with respect to the data for the following night although it gives a similar slope and, therefore, similar results in Table 4. This effect is presumably due to the extreme blueshifts measured near $\varphi \sim 0.0$ on June 25 and the change of slope near the end of the event on the same night, which coincides with a transient chromospheric brightening. The fact that $H\alpha$ emission is also enhanced at the closing phases on June 27 (**a₂₇** in Fig. 4) suggests a possible activation of the plage region at the end of its disk transit. Evidence of sudden brightening at these phases is also seen in the Ca II and He I D₃ lines. Because the same effect has been detected on different nights and has a short duration, it cannot be attributed to a flare. An alternative explanation could be in terms of an *active longitude* at which the emission feature **a** is enhanced. It would be very interesting to investigate spot activity on this star and study the distribution of its spots in order to support this idea. Observational evidence for preferential longitudes favouring spot and

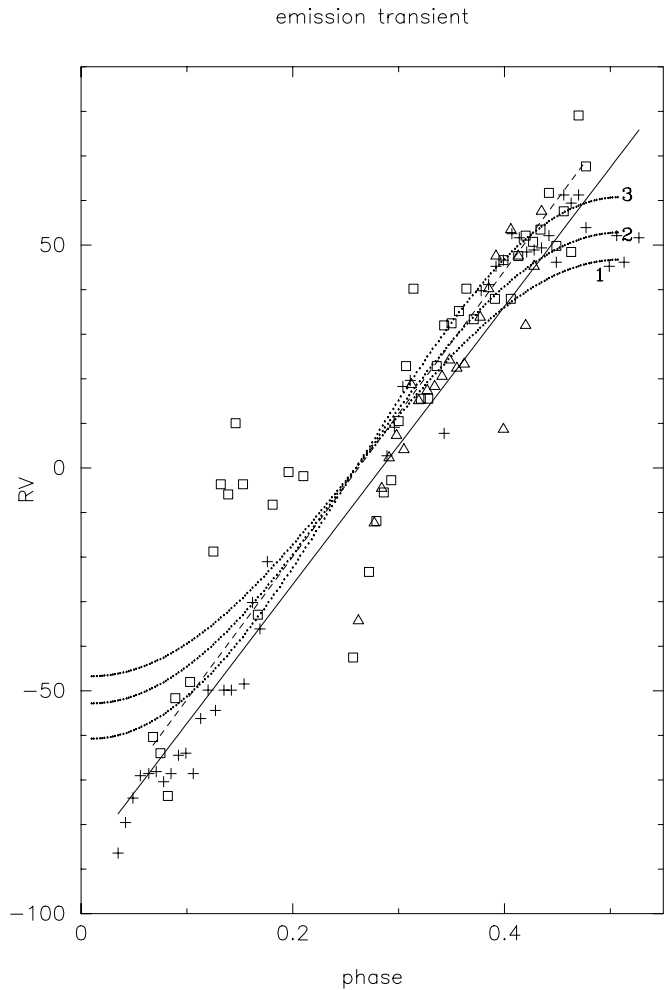


Fig. 15. Observed variation of the plage radial velocity (RV) with phase for the nights 25 June (+), 26 June (□), 27 June (△). The straight lines are the linear fits for the nights on which reasonable coverage of the transient was achieved: 25 June (—) and 26 June (- -). For comparison, predicted radial velocity curves of an absorbing point-like source in co-rotation with the star at distances close to the surface are overplotted. Note that radial velocities are always relative to the stellar centre of mass. Three different cases were considered, varying the height (R) and the co-latitude (θ) of the feature: $R=1.0R_*$, $\theta=50^\circ$ (*curve 1*); $R=1.0R_*$, $\theta=60^\circ$ (*curve 2*); $R=1.3R_*$, $\theta=50^\circ$ (*curve 3*)

chromospheric activity has been reported in Fernández & Miranda (1998).

8. Conclusions

A detailed analysis of the $H\alpha$ emission line variability in RE 1816+541 was first aimed at seeking evidence for the phe-

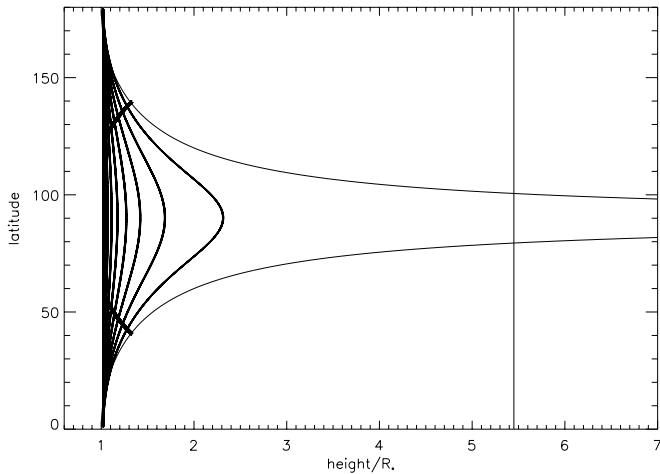


Fig. 16. Same as Fig. 14 but for the plage-like region observed on RE 1816+541. The two thin contours show the possible solutions for the height and latitude of the feature in the stellar atmosphere, using data for the nights of June 25 and June 26 (see Table 4)

nomenon of stellar prominences in this object. Results presented here have clearly demonstrated that prominence clouds exist and are seen to lie below the co-rotation radius. In this respect, prominences in RE 1816+541 are more similar to HK Aqr's (Byrne, Eibe & Rolleston 1996) prominences than to AB Dor's prominences (Cameron & Robinson 1989a,b). This suggests that the role of stellar prominences in carrying away angular momentum from the star may be not so significant as it was initially thought.

Some of the variations, however, show a very complex behaviour and the only way to understand completely their nature would be to obtain more continuous observations. In addition, strong emission transients are seen to occur very frequently, making the study of these events more difficult. One of such emission transients was well covered on the three nights of observations and provided evidence for surface active regions which, by virtue of the star's rapid rotation, could be mapped on its chromosphere. More information about their size and physical state could be obtained from Doppler imaging techniques.

Acknowledgements. Most of this research has been done under supervision by Dr. P.B. Byrne at Armagh Observatory. His untimely death occurred before this work was completed. It has been a sad end for a project that benefited so much from his enormous help and encouragement. Research at Armagh Observatory is grant-aided by the Dept. of Education for Northern Ireland. Support staff of the WHT (La Palma) is gratefully acknowledged for their assistance during the observations. This work has also benefited from the STARLINK project funded by the UK PPARC. The author acknowledges a PPARC Research Studentship No. 9400747X during the period of this work. The author would like to thank all the staff in LAEFF for their kind support during the last steps of this work, particularly Dr. B. Montesinos for his help and careful reading of the manuscript. The author also wishes to thank the referee of this paper, Dr. A. Collier-Cameron, for helpful comments.

References

- Basri, G., Marci, G.W. 1995, *AJ*, 109, 762
 Byrne, P.B., Eibe, M.T., Rolleston, W.R.J. 1996, *A&A*, 311, 651
 Caillault, J.P., Patterson, J. 1990, *AJ*, 100, 3, 825
 Cameron, A.C., Robinson, R. 1989a, *MNRAS*, 236, 57
 Cameron, A.C., Robinson, R. 1989b, *MNRAS*, 238, 657
 Collier-Cameron, A. 1988, *MNRAS*, 233, 235
 Collier-Cameron, A., Jianke, L. 1994, *MNRAS*, 269, 1099
 Collier-Cameron, A., Woods, J.A. 1992, *MNRAS*, 258, 360
 Collier Cameron, A., Duncan, D.K., Ehrenfreund, P., Foing, B.H., Kuntz, K.D., Penston, M.V., Robinson, R.D., Soderblom, D.R. 1990, *MNRAS*, 247, 415
 Demircan, O., Kahraman, G. 1991, *Ap&SS*, 181, 313
 Eibe, M.T. 1997, in *Prominences on active late-type stars*, PhD-thesis in Physics, Queen's University of Belfast
 Fernández, M., Miranda, L.F. 1998, *A&A*, 332, 629
 Henry, T.J., McCarthy, D.W. 1993, *AJ*, 106, 2, 773
 Jeffries, R.D. 1993, *MNRAS*, 262, 369
 Jeffries, R.D., James, D.J., Bromage, G.E. 1994, *MNRAS*, 271, 476
 Jenkner, H., Lasker, B., Sturch, C., McLean, B., Shara, M., Russell, J. 1990, *AJ*, 99, 2082
 Parker, E.N. 1970, *ARA&A*, 8, 1
 Robb, R.M., Cardinal, R.D. 1995, *IBVS*, 4270
 Schwartz, R.D., Dawkins, D., Findley, D., Chen, D. 1995, *PASP*, 107, 667
 Stauffer, J.R., Hartmann, L., Soderblom, D.R., Burnham, N. 1984, *ApJ*, 280, 202
 Stauffer, J.R., Hartmann, L., Burnham, N., Jones, B.F. 1985, *ApJ*, 289, 247
 Tody, D. et al. 1986 *IRAF User's Manual*, National Optical Astronomical Observatories.
 Unger, S., Pettini, M. 1993, *UES User's Manual*. Isaac Newton Group, La Palma.
 van den Oord, G.H.J. and Zuccarello, F. 1996, in *IAU Symp. 176 'Stellar Surface Structure'*, eds. Strassmeier, K.G., Linsky, J.L., Kluwer, p. 433
 van den Oord, G.H.J., Eibe, M.T., Byrne, P.B. 1998, *A&A*, submitted (VEB98)